Supporting Information

Rational Design of Solid-Acid Catalysts for Cellulose Hydrolysis Using Colloidal Theory

Ziyang Zhang,[†] Geoffrey A. Tompsett,[†] Sergio Granados-Focil,[*] Christopher R. Lambert,[#] Michael T. Timko[†]

[†] Department of Chemical Engineering, Worcester Polytechnic Institute MA 01609, United States

[#] Department of Chemistry & Biochemistry, Worcester Polytechnic Institute MA 01609, United States

[*] Department of Chemistry, Clark University Worcester, MA 01610, United States

Table of content

List of Symbols

U	DLVO total interaction energy (J)
U_{VDW}	van der waals attraction energy (J)
U_{EDL}	Electrical double layer interaction energy (J)
A_{132}	Hamaker constant of cellulose (1) interacting with catalyst (2) across water (3) (J)
A_{11}	Hamaker constant of cellulose-cellulose interaction in vacuum (J)
A_{22}	Hamaker constant of catalyst-catalyst interaction in vacuum (J)
A_{33}	Hamaker constant of water-water interaction in vacuum (J)
R_1	Radius of cellulose particle
R_2	Radius of catalyst particle
x	Cellulose-catalyst separation
k_b	Boltzmann constant, 1.38×10^{-23} $(J\,K^{-1})$
T	Temperature (K)
ε_i	Relative permittivity of cellulose (ε_1), catalyst (ε_2), water (ε_3) and free space (ε_0)
n_i	Refractive index of cellulose (n_1), catalyst (n_2), water (n_3)
h	Planck constant (J.s)
v_e	Rotational frequency (s^{-1})
ψ	Electrical potential (V)
ψ_0	Surface electrical potential (V)
c	Ions number concentration (L^{-1})

z	Valence number
e	Electron charge, 1.60×10^{-19} (C)
κ	Reciprocal of Debye length (m⁻¹)
λ_D	Debye length (m)
Z	Zeta potential (V)
k_a	Acid dissociation constant
k_b	Base dissociation constant
Γ_{AH}	Surface coverage of undissociated acid (mol m⁻²)
Γ_{BOH}	Surface coverage of undissociated base (mol m⁻²)
Γ_{A^-}	Surface coverage of dissociated acid A⁻ (mol m⁻²)
Γ_{B^+}	Surface coverage of dissociated acid B⁻ (mol m⁻²)
Γ_{At}	Total acid surface coverage (mol m⁻²)
Γ_{B_t}	Total acid surface coverage (mol m⁻²)
σ_0	Surface charge density (C m⁻²).

1. Supplemental Figure

Figure SI-1 indicates that the field grew rapidly between 2007-2014, reaching a steady value between 50 and 80 publications per year from 2014-2019. The result is that the field has expanded from a handful of publications in 2007 to a cumulative total of more than 500 over a 13-year time period.
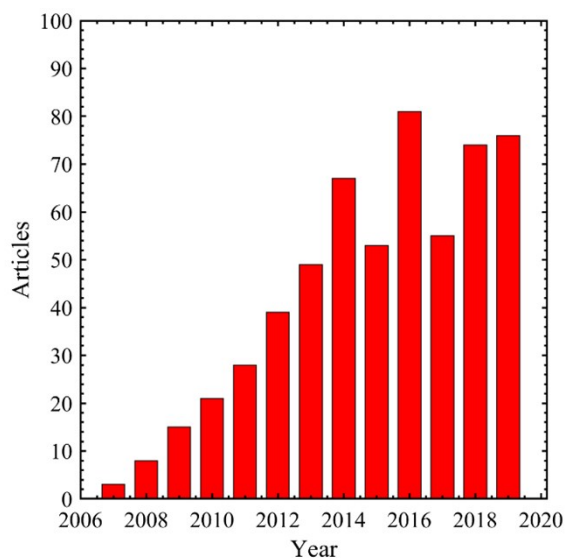
Figure SI-1 shows the number of annually published articles since 2006. The data was obtained from Web of Science with the search keywords "solid acid catalyst cellulose hydrolysis".

2. DLVO Theory Section

DLVO theory, named after Boris Derjaguin and Lev Landau, Evert Verwey and Theodoor Overbeek, forms the basis of understanding whether colloidal particles will agglomerate or remain dispersed when in solution. DLVO theory divides colloidal interactions into a van der Waals component and an electrical double layer component:[1]

$$U = U_{VDW} + U_{EDL}$$

[1]

where U is the total DLVO interaction energy, U_{VDW} is the interaction energy arising from van der Waals force and U_{EDL} represents the interaction energy of electrostatic double-layer force.

The van der Waals interaction energy (U_{VDW}) between two spherical particles follows a power law with respect to particle-particle separation (x), as derived by Hamaker:[1]

$$U_{VDW}(x) = -\frac{A_{132}}{6}\left[\frac{2R_1 R_2}{x(2R_1 + 2R_2 + x)} + \frac{2R_1 R_2}{(2R_1 + x)(2R_2 + x)} + ln\frac{(2R_1 + 2R_2 + x)x}{(2R_1 + x)(2R_2 + x)}\right]$$

[2]

A_{132} is the combined nonretarded Hamaker constant for cellulose-solid-acid catalyst interacting across water. For the purposes of this study, cellulose is denoted as "1", the solid-acid catalyst is denoted as "2", and the solvent (water) is denoted as "3". The value of A_{132} can be determined by empirical data fitting or (more typically) can be estimated using a combinatorial rule:[2]

$$A_{132} = -\left(\sqrt{A_{11}} - \sqrt{A_{33}}\right)\left(\sqrt{A_{22}} - \sqrt{A_{33}}\right)$$

(3)

where A_{11} is the Hamaker constant of cellulose-cellulose interacting across vacuum, A_{22} denotes the Hamaker constant for catalyst-catalyst interaction, and A_{33} is the Hamaker constant of water interacting with itself.

Values of individual Hamaker constants (A_{ii}) can be obtained by fitting force-distance data, which is time-consuming and instrument-dependent. Instead, the approach recommended by Lifshitz [2] can be adopted to estimate A_{ii} based on values of dielectric constant and refractive index, both of which are commonly available. The expression is given as:

$$A_{ii} = \frac{3}{4}k_b T\left(\frac{\varepsilon_i + 1}{\varepsilon_i - 1}\right)^2 + \frac{3hv_e}{16\sqrt{2}}\frac{(n_i^2 - 1)^2}{(n_i^2 + 1)^{3/2}} \tag{4}$$

where v_e is the main electronic absorption frequency in the ultraviolet region, typically around $3 \times 10^{15}\ s^{-1}$. Equation (4) indicates that the interaction is always attractive for particles with identical permittivity and refractive index. [1] Appropriate values for the index of refraction and dielectric constant are available in the literature for cellulose and model materials representative of major catalyst types (e.g., oxides, carbon, and polymers).

The second term in the overall DLVO interaction energy arise from electrostatic interaction, which can either result in repulsion or attraction, depending on the charges sign of the two examined surfaces relative to one another. Cellulose and most catalyst materials, especially those bearing acid groups, are negatively charged when placed in aqueous solutions, either due to dissociation of ionizable functional groups or adsorption of ions.[3] To quantify the electrostatic repulsion, the electrical potential distribution between the particles must be computed using the Poisson-Boltzmann (P.B.) distribution:[4]

$$\nabla^2\psi = \frac{8\pi cez}{\varepsilon_0\varepsilon_3}sinh\boxed{}(\frac{ze\psi}{k_bT})$$

(5)

For spherical particles, the PB equation reduces to:[4]

$$\frac{d^2\psi}{dx^2} = \kappa^2\psi$$

(6)

where κ is reciprocal of the Debye length, which characterizes the thickness of the diffusion layer and which varies from a few hundred nanometers in pure water to several nanometers in highly concentrated ion solutions. The Debye length is defined as:

$$\kappa = \lambda_D^{-1} = \sqrt{\frac{\sum(z_ie)^2c}{\varepsilon_0\varepsilon_3k_bT}}$$

(7)

where all terms have been defined previously.

Solution of the P.B. equation gives the electrical potential as a function of radial distance (x) from the surface. Many mathematical methods, both numerical and analytical, have been developed to solve the P.B. equation.[5] Among these mathematical methods, Hogg at al. provided an analytical solution appropriate for spherical particles.[4] The expression for U_{edl} given by the Hogg solution of the PB equation is shown as equation (8):

$$U_{EDL}(x) = \frac{\varepsilon_0\varepsilon_3R_1R_2(\psi_{01}^2 + \psi_{02}^2)}{4(R_1 + R_2)}\left[\frac{2\psi_{01}\psi_{02}}{(\psi_{01}^2 + \psi_{02}^2)}\ln\left(\frac{1 + \exp(-\kappa x)}{1 - \exp(-\kappa x)}\right) + \ln(1 - \exp(-2\kappa x))\right]$$

(8)

Inserting Equations (2) and (8) into Equation (1) allows calculation of U as a function of particle-particle separation.

3. Hamaker constant (A_{132}) Determination Section

The vdw interaction always exists between particles, and its magnitude is determined primarily by the value of the nonretarded Hamaker constant, a quantity that is typically determined by fitting force-distance curve for interacting particles. Accurate estimation of Hamaker constant would facilitate us evaluate the reported catalysts and also identify potential catalysts candidate for cellulose hydrolysis.

Lifshitz theory (Eqn. 4) that use optical properties such as dielectric constant and refractive index has provided accurate estimation for a wide range of particles interaction in polar solvents such as water. Accordingly, dielectric constant and refractive index for cellulose and some common catalysts substrate materials, including carbon, iron oxide, zirconia, polystyrene and Nafion are extracted from literatures (table SI-1). Then Hamaker constant (A_{ii}) for individual materials interacting with itself across the vacuum is obtained using equation (4). Then equation (3) is being utilized to compute nonretarded Hamaker constant for cellulose-catalyst interaction in aqueous solution. The computed Hamaker constant (A_{132}) for cellulose and solid-acid catalysts are not generally available in literature. A_{ii} is compared with literature value where available. For example, the calculated Hamaker constant of cellulose interacting with itself in vacuum is approximately 6.4×10^{-20}J, which is close to 5.8×10^{-20} J reported by Bergström et al. using spectroscopic ellipsometry.[6] Hough and White use the exact solution of the Lifshitz theory to compute A_{132} for zirconia and obtain 20×10^{-20}J, which close to the value in **Table SI-1**. Reported A_{ii} using "Quasi-Dynamic" method for polystyrene is about 7.9×10^{-20}J and close to 8.30×10^{-20}J.[88] Literature reported Hamaker constant for magnetite is about 40×10^{-20}J and is higher that calculated value (34.8×10^{-20}). Although the accuracy of Hamaker constant obtained from different physical instruments is still in debate, the Lifshitz theory still remains the

most widely used theoretical approach to estimate Hamaker constant. The congruence of calculated Hamaker constant with literature values suggests the promise of Lifshitz theory for determining A_{132} without involving experimental efforts.

Table SI-1. Calculated Hamaker constant ($\times 10^{-21}$ J) for different solid-acid catalysts interacting with cellulose in water using Lifshitz theory

Materials	n_i	ε_r	A_{ii}	A_{132}	Ref.
Cellulose	1.53	7.6	64.0	-	[7, 8]
Carbon	2.42	12	439	36.0	[9, 10]
Fe_3O_4	2.42	8.5	348	35.0	[11]
ZrO_2	2.15	18	262	28.8	[12, 13]
Polystyrene	1.55	2.6	83	10.7	[14]
Nafion	1.38	3.5	103	1.70	[15]

The data provided in **Table SI-1** suggest that Hamaker constant (A_{132}) for cellulose-catalysts interaction across water (A_{132}) increases in the sequence of: activated carbon $> Fe_3O_4 > ZrO_2 >$ polystyrene >Nafion, ranging from 0.17×10^{-20} J to 3.60×10^{-20} J. Interestingly, carbon and metal oxides e.g. Fe_3O_4 and ZrO_2 are excellent candidates for adsorbing cellulose. This is in accord with the fact that carbon materials and metal oxides are protons donors because of its rich electron cloud density, resulting in strong vdw attraction. [16] Not surprisingly, increasing the catalyst surface electron density has been a widely used approach to tailor catalyst catalytic performance. [17] In contrast, polymer materials such as Nafion are chemically inert and have low tendency to adsorb cellulose. Polystyrene has an intermediate Hamaker constant (A_{132}) of

1.07×10^{-20} J, allowing it having greater attraction than Nafion with cellulose. The catalysts showing in **Table SI-1** cover three main categories, including carbon, polymer, metal oxides solid materials. However, this does not necessarily represent all the catalysts within each category. In fact, even for the case of metal oxides, the Hamaker constant (A_{ii}) can vary drastically. [18] In evaluating individual catalyst vdw attraction, accurate optical properties such as dielectric constant refractive index should be obtained for the accurate prediction of Hamaker constant.

4. Estimating Surface Potential of Bifunctional Catalysts

The surface of a solid catalyst particle will become charged upon aqueous immersion due to acid dissociation and subsequent ion adsorption. The charge density of the surface depends on several factors, including catalyst acidity (*pKa*), catalyst surface acid density, and solution *pH* or ionic strength.[19]

The charge density/surface potential can be rendered in terms of measurable parameters, e.g. *pKa*, *pH* and acid surface coverage, either using experimental measurements of the zeta potential (ζ) or a mathematical model that can predict surface acid dissociation. In the first of these, the zeta potential is an indirect measure of the surface potential, and the two quantities can be related to one another using the following expression:[2]

$$\psi_0 = \frac{4k_bT}{ze}\tanh^{-1}(tanh(\frac{ze\zeta}{4k_bT}) \times e^{\kappa d})$$

(9)

where *d* is the distance between particle surface and slipping plane, often taking the value of 5-6 Å. [2] In principle, ζ is a function of *pH* and possibly ionic strength. Here, we will use equation (9) and *pH* resolved measurements of ζ to approximate ψ_0 for particles that have published data, namely cellulose, zirconia, Nafion, and activated carbon.

When experimental ζ measurements are not available, a second method can be used to relate surface acid density and pKa (or pKb)to surface potential. [19] For a bifunctional catalyst bearing acid groups (*AH*) and base groups (*BOH*), the surface can be charged either by deprotonation of *HA* or protonation of *BOH*:

$$AH \rightleftarrows H^+ + A^- \tag{10}$$

$$BOH \rightleftarrows OH^- + B^+ \tag{11}$$

Two assumptions can be applied to simplify the model: I). ionization of individual sites are independent of one another and do not interact with each other; ii). protonation of *HA* occurs only under extremely acidic condition (typically $pH < 1$,) that are not of interest here.

With these two assumptions, dissociation can be quantified by the equilibrium dissociation constant (Ka and K_b):

$$K_a = \frac{[H^+]_0 \Gamma_{A^-}}{\Gamma_{AH}} \tag{12}$$

$$K_b = \frac{[OH^-]_0 \Gamma_{B^+}}{\Gamma_{BOH}} \tag{13}$$

where $[H^+]_0$ is the protons activity around solid-acid catalyst surface and $[OH^-]_0$ is the hydroxide ions activity around surface. Γ_{AH} is surface acid density for undissociated acid and Γ_{A^-} is the surface density for dissociated acid or substrate catalyst, and the same definition applies to *BOH*.

Applying the P.B. distribution equation, the proton activity around the solid surface and that in bulk phase can be correlated as:[19]

$$[H^+]_0 = [H^+]_b \, exp(-\frac{e\psi_0}{k_b T})$$

(14)

where $[H^+]_b$ is the proton activity in bulk phase, and it is normally determined by measuring solution *pH*.

When placed in a solution with *pH* > pKa, the surface will become negatively charged, resulting in a non-zero value of the surface charge density (σ_0):

$$\sigma_0 = eN_A \left\{ \Gamma_{B^+} - \Gamma_{A^-} \right\}$$

(15)

The surface acid coverage can then be related to the dissociated acid surface concentration. The total acid concentration consists of dissociated and undissociated site density for both acid head group and substrate catalysts and is given by:[19]

$$\Gamma_{A_t} = \Gamma_{AH} + \Gamma_{A^-}$$

(16)

$$\Gamma_{B_t} = \Gamma_{BOH} + \Gamma_{B^+}$$

(17)

Equations (10-17) can be solved for surface charge density as a function of measurable quantities, including *pH*, *pKa*, surface coverage (Γ_{tot}). However, upon solving the above equations, surface charge density and surface potential are inter-correlated. Obtaining separate equations for surface potential and density individually requires a separate equation. Here, the Grahame equation will be used to relate surface charge density to surface potential, since it is appropriate for curved surfaces: [20]

$$\sigma_0 = \frac{\varepsilon_0 \varepsilon_3 \kappa k_b T}{2\pi e} [\sinh\left(\frac{e\psi_0}{2k_b T}\right) + \frac{2}{\kappa a} tanh(\frac{e\psi_0}{4k_b T})]$$

(18)

where ε_0 is the vacuum permittivity and ε_3 represents the dielectric constant of water, κ is the reciprocal of Debye length, k_b is the Boltzmann constant and ψ_0 is the surface potential. Solving Equations (10-18) simultaneously allows explicit determine of either the surface potential (ψ_0) or surface charge density (σ_0),.

In practice, the approach based on Equations (10-18) works best for materials bearing well-defined acid groups. Here, we apply the second approach to functionalized ZSM catalysts bearing carboxylic/sulfonic acid functionalized catalysts, and Nafion materials where surface acid coverage and acid the dissociation equilibrium constant are accurately known. (**Figure 2b** and **Figure 2d**). The few cases where the surface acid coverage and dissociation constant are both known and where pH-resolved measurements of ζ are available permit direct comparison.

To demonstrate this method, we have selected ZSM-5 as an example as substrate materials and assume it bears three acid groups with p*Ka* of 2.5, 1.0 and -2. The predicted surface potential results as a function of *pH* are show in **Figure SI-2**. Overall, predicted surface potential of ZSM-5 bearing acid group increases as *pH* increases, in accord with the fact that the anions can attract counter-ions at high ionic strength aqueous solution and reduce the surface charge density or surface potential. In particular, this localized protonation becomes significant for weak acid. For strong acid such as sulfonic aid with pKa smaller than -2, the surface potential is somehow insensitive to *pH* change and stays relatively constant around -230 mV, as shown in **Figure SI-2**. Predicted surface potential for weak acid (e.g. carboxylic acid with pKa around 2.5) varies from close to zero at low *pH* (around 1) to around -170V at *pH* close to 6. The change of surface potential with respect to *pH* is steeper at pH between 2-3 and reaches to flat at pH about 5. For acid with intermediate strength (pKa = 1), the variation of the surface potential over pH between 1 and 6

follows the same trend as the cases for weaker acid (e.g. pKa = 2.5). Overall, the predicted surface

potential captures.
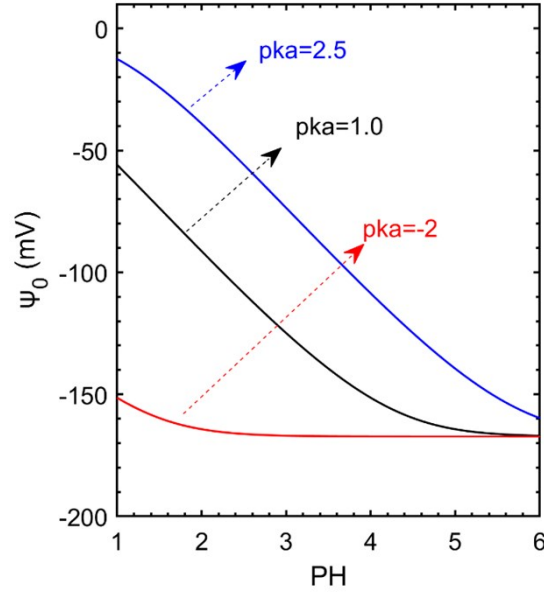
Figure SI-2 The surface potential of ZSM-5 bearing different acid head group as a function of

media *pH*. The p*Ka* of acid head group is taken as 2.5, 1.0 and -2 from weak acid to strong acid.

The pK_b for the base group is assumed as 8.0. The substrate (ZSM-5) surface density is assumed

as 5.0 nm^{-2}. Particle size is assumed as 1 μm.

5. Shear Force Effect on Cellulose-Catalyst Aggregation

Shear-induced aggregation is discussed and derived by Zaccone et al.[21] as a shear rate-

dependent Arrhenius equation for aggregation rate constant of two-body particle interaction:

$$k_{ij} = \sqrt{\frac{3\pi\alpha u \gamma (R_i + R_j) R_i R_j - U_m''|_{xm}}{k_B T}} e^{[-U_m + 6\pi u \gamma (R_i + R_j) R_i R_j]/k_B T} \tag{19}$$

where k_{ij} is coagulation rate constant, u is viscosity, γ is shear rate, U_m is DLVO energy barrier and $U_m''|_{xm}$ is the second derivate of U_m with respect to separation (x) evaluated at DLVO energy barrier.

The activation energy for shear-induced aggregation takes the form of:

$$E_a = \frac{\left[-U_m + 6\pi u\gamma(R_i + R_j)R_iR_j \right]}{k_BT} \tag{20}$$

In the case where shear force counterbalances DLVO energy barrier and diminish the barrier, this critical shear rate is an important condition defining the transition from slow aggregation to fast aggregation[21]. Thus, the critical shear rate becomes:

$$\dot{\gamma}^* = \frac{U_m}{6\pi u(R_i + R_j)R_iR_j} \tag{21}$$

For a specific solid catalyst with fixed Hamaker constant, the energy barrier (U_m) is strongly dependent on surface potential and particle size. To capture this effect, the surface potential of the solid catalyst is systematically varied from 0 mV to −120 mV for catalyst radius of 0.5, 1, 1.5 and 2 μm. Then equation (1) is used to determining the maximum energy barrier for specific surface potential and catalyst radius. Finally, equation (21) is employed for calculating critical shear rate.

In a typical hydrolysis setup, a magnetic stirring bar is inserted into a 15-mL heavy wall glass tube (ChemGlass LLC.). The stirring speed, which affects the shear flow of the reaction medium, is often set in the rage of 200-800 rpm. For simplification, we assume that the stirring bar can be modeled as a cylinder that is concentric with the reaction vessel, with fluid confined to the annulus.[22] Figure SI-3 shows the schematic. The annular geometry will tend to overestimate the average shear rate in the reactor; accordingly, we focus our analysis on the maximum shear

rate, which should be captured with reasonable accuracy using the geometry shown in Figure SI-3.
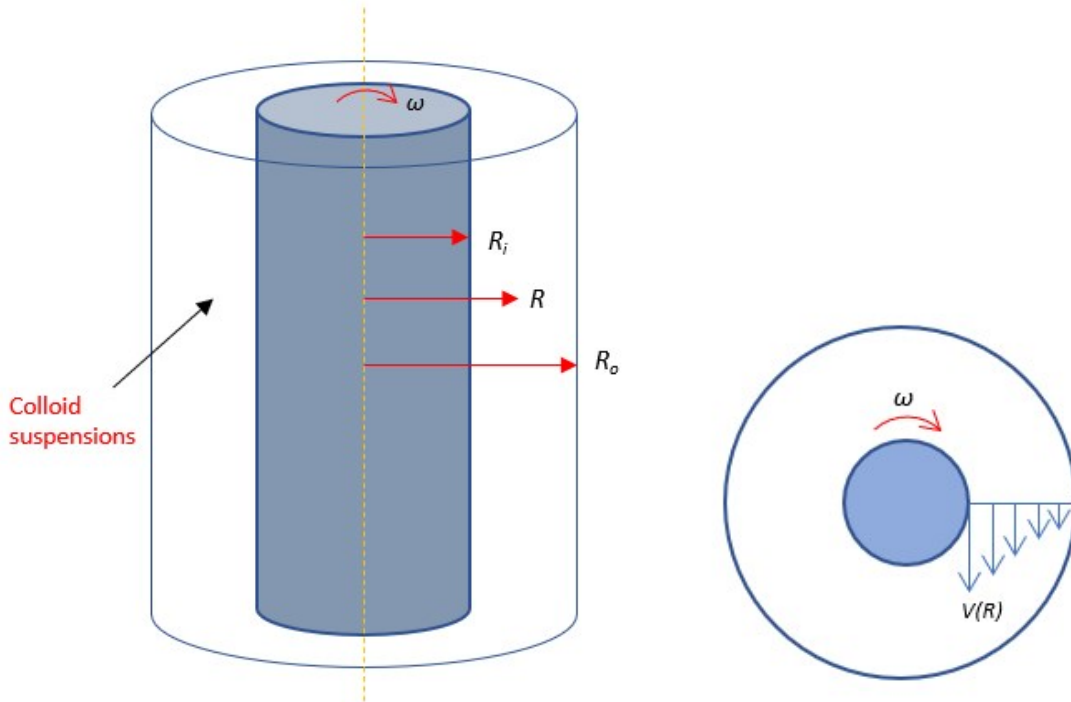
Figure SI-3 Schematic of reaction system of lab-scale batch reactor for cellulose hydrolysis. Left

is the side view of the glass tube reactor and right is top view for velocity profile.

The velocity profile is given by:

$$v(R) = \frac{\omega R_i^2}{R_o^2 - R_i^2}(\frac{R_o^2}{R} - R)$$

(22)

where ω is angular velocity of the inner cylinder (or the rotating speed of stirring bar), R_i and R_o

are radius of inner and outer cylinders respectively, R is an arbitrary radius.

Therefore, the corresponding shear rate between the moving fluid and stationary cylinder is:

$$\gamma(R) = \frac{\omega R_i^2}{(R_o^2 - R_i^2)(R_o - R)} \left(\frac{R_o^2}{R} - R \right) \quad R_i < R < R_o \tag{23}$$

Equation (23) will be used to extract shear rate profile along the radial direction. Notice that equation (23) can apply to the shear rate at glass tube (e.g. $R = R_o$) because of the denominator term $(R_o\text{-}R)$. Figure SI-4 shows some representative shear rate when the inner cylinder (or the stirring bar) rotates at the speed of 200, 400, 600 and 800 rpm. In general, the shear rate is maximized in the center of the reactor and then it decreases nonlinearly along outward radial direction. The maximum shear rate is reported in the text at representative stirring rates (200 and 800 rpm).
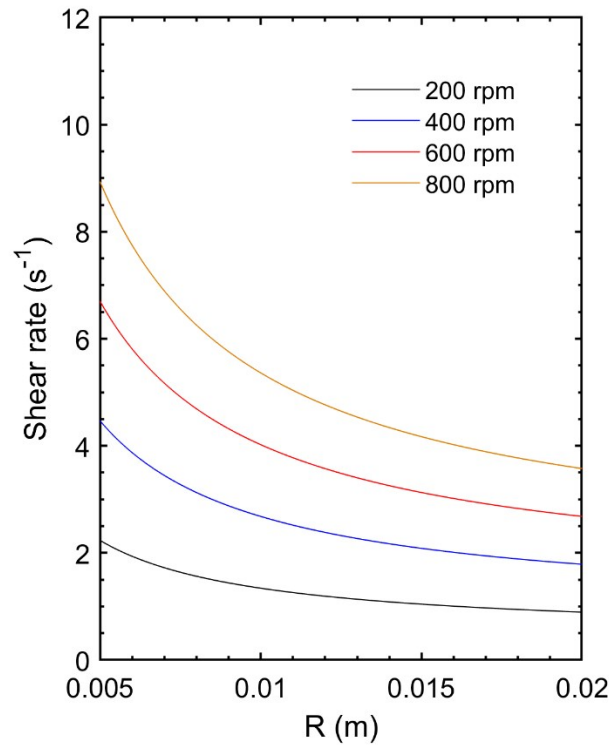
Figure SI-4 Shear rate distribution within glass tube reactor. R_o is assumed as 2 cm and inner cylinder radius R_i is 0.5 cm.

6. Temperature Effect on Cellulose-Solid-Acid Interactions

Most reported hydrolysis reaction are performed within the temperature range of 350-450K. Under mildly high temperature, the first order effect of changing temperature is from thermal fluctuations, which is easily accounted for using $k_b T$ in the DLVO analysis. And the particle-particle collisions changes caused by raising temperature is negligible considering the hydrodynamics friction is large enough to reduce thermal fluctuation.

A secondary direct effect is the dependence of the Hamaker constant and surface potential on changing temperature. The van der Waals attraction is caused by electronic fluctuation, and it is weakly dependent or independent on external temperature fluctuations. Therefore, van der Waals attraction between cellulose and solid acid is relatively constant under given reaction condition. The effect of temperature on catalyst surface potential/charge density is much more complicated to consider. First, temperature affect water dielectric and ionization constants (ε and K_w). In fact, the dielectric constant varies from 78 at 25 °C to approximately 35 at 200 °C, the upper range of temperatures used for catalytic cellulose hydrolysis.[23] As a result, Debye length will increase and water will be much less effective at screening charges than room temperature water, enhancing electrostatic repulsion and resulting in net colloidal stabilization for similarly charged particles. Second, water ionization constant (K_w) increase from 1×10^{-14} to 1×10^{-11} when water is heated from 25 to around 200 °C, with the net effect being to adjust protonation/deprotonation equilibria, especially for weak acids and bases. Comparatively, the dissociation constants[24] of carboxylic acids – and probably sulfonic acids – are much weaker functions of temperature than water over the same temperature range. Accordingly, the main effect of temperature on acid-base interactions should be due to the temperature dependence of water dissociation. Lastly, despite that increasing temperature may enhance the acid dissociation, resulting in higher ionic strength than at room temperature. This increased ionic strength may

contribute to the aggregation; however, this would largely depend on how sensitive the acid dissociation to temperature and whether it is endothermal or exothermal reaction. Therefore, the effect of temperature on electrostatic interaction is complicated to consider.

To simplify the temperature effect, we have taken dielectric constant of water, cellulose and solid-acid catalyst (e.g. carbon, zirconia and polystyrene) under different temperature and substitute those into equations(1-8). The results and analysis are provided in the manuscript.

7. Solvent Effect on Cellulose-Solid-Acid Interaction

Heating water to temperatures greater than 100 °C has been compared with the effect of changing solvents;[25] Accordingly, an alternative strategy for manipulating catalyst-cellulose binding is to change the solvent entirely. Various alcohol water mixtures,[26] tetrahydrofuran-water mixtures,[27] and mixtures of g-Valero lactone and water [28] have been suggested for biomass deconstruction solvents, and combining non-aqueous solvents with solid acid catalysts may provide substantial technological benefits. Unfortunately, colloidal stability in non-aqueous solvents has been the subject of limited studies, meaning that more work is required to arrive at definitive conclusions.

From the considerations presented here, a first order effect of changing solvent will (generally) be to decrease the dielectric constant, accentuating both attractive and repulsive electrical double layer interactions and with only a handful of exceptions for unusual solvents, such as formamide (e = 109.5) or methylformamide (e = 182.4).[29] Accordingly, negatively charged solid acids will more strongly repel negatively charged cellulose in non-aqueous solvents than in water, assuming that the values of the surface potentials themselves are not changed when the solvent is switched. That stated, non-aqueous solvents will shift acid-base dissociation equilibrium to favor the neutral forms of acids and bases compared with water, meaning that the

assumption of constant surface potential is likely erroneous and instead absolute values of the

surface potential will be less in non-aqueous solvents than in water. Similarly, the activity of the

proton itself is greater in non-aqueous solvents than in water,[30] meaning that combining the other

strategies presented here – manipulating particle size, maximizing Hamaker constant, and using

bifunctional catalysts to control surface potential – with use of non-aqueous solvents has potential

to open entirely new avenues.

Reference

1. Israelachvili, J.N., *Intermolecular and surface forces*. 2011: Academic press.
2. Van Oss, C.J., M.K. Chaudhury, and R.J. Good, *Interfacial Lifshitz-van der Waals and polar interactions in macroscopic systems.* Chemical reviews, 1988. **88**(6): p. 927-941.
3. Duro, R., et al., *The adsorption of cellulose ethers in aqueous suspensions of pyrantel pamoate: effects on zeta potential and stability.* European journal of pharmaceutics and biopharmaceutics, 1998. **45**(2): p. 181-188.
4. Hogg, R., T.W. Healy, and D.W. Fuerstenau, *Mutual coagulation of colloidal dispersions.* Transactions of the Faraday Society, 1966. **62**: p. 1638-1651.
5. Derjaguin, B., *A theory of the heterocoagulation, interaction and adhesion of dissimilar particles in solutions of electrolytes.* Discussions of the Faraday Society, 1954. **18**: p. 85-98.
6. Bergström, L., et al., *Spectroscopic ellipsometry characterisation and estimation of the Hamaker constant of cellulose.* Cellulose, 1999. **6**(1): p. 1-13.
7. Shimazaki, Y., et al., *Excellent thermal conductivity of transparent cellulose nanofiber/epoxy resin nanocomposites.* Biomacromolecules, 2007. **8**(9): p. 2976-2978.
8. Stoops, W., *The dielectric properties of cellulose.* Journal of the American Chemical Society, 1934. **56**(7): p. 1480-1483.
9. Shkal, F., et al., *Microwave characterization of activated carbons.* Journal of Computer and Communications, 2017. **6**(1): p. 112-123.
10. Dore, P., et al., *Infrared properties of chemical-vapor deposition polycrystalline diamond windows.* Applied optics, 1998. **37**(24): p. 5731-5736.
11. Ansar, M., et al., *Frequency and temperature dependent dielectric response of Fe 3 O 4 Nano-crytallites.* Journal of Scientific Research, 2014. **6**(3): p. 399-406.
12. Harrop, P. and J. Wanklyn, *The dielectric constant of zirconia.* British Journal of Applied Physics, 1967. **18**(6): p. 739.
13. Wood, D.L. and K. Nassau, *Refractive index of cubic zirconia stabilized with yttria.* Applied Optics, 1982. **21**(16): p. 2978-2981.
14. Ghosh, G., *Dispersion-equation coefficients for the refractive index and birefringence of calcite and quartz crystals.* Optics communications, 1999. **163**(1-3): p. 95-102.
15. Majsztrik, P.W., A.B. Bocarsly, and J.B. Benziger, *Viscoelastic response of Nafion. Effects of temperature and hydration on tensile creep.* Macromolecules, 2008. **41**(24): p. 9849-9862.

16.   Hasan, Z., et al., *Preparation of calcined zirconia-carbon composite from metal organic frameworks and its application to adsorption of crystal violet and salicylic acid.* Materials, 2016. **9**(4): p. 261.

17.   He, D., et al., *Active Electron Density Modulation of Co3O4-Based Catalysts Enhances their Oxygen Evolution Performance.* Angewandte Chemie, 2020. **132**(17): p. 6996-7002.

18.   Lefevre, G. and A. Jolivet. *Calculation of Hamaker constants applied to the deposition of metallic oxide particles at high temperature*. in *Proceedings of International Conference on Heat Exchanger Fouling and Cleaning*. 2009.

19.   Behrens, S.H. and D.G. Grier, *The charge of glass and silica surfaces.* The Journal of Chemical Physics, 2001. **115**(14): p. 6716-6721.

20.   Russel, W.B., et al., *Colloidal dispersions*. 1991: Cambridge university press.

21.   Zaccone, A., et al., *Theory of activated-rate processes under shear with application to shear-induced aggregation of colloids.* Physical Review E, 2009. **80**(5): p. 051404.

22.   Wang, H., *Experimental and numerical study of Taylor-Couette flow.* 2015.

23.   Akerlof, G., *Dielectric constants of some organic solvent-water mixtures at various temperatures.* Journal of the American Chemical Society, 1932. **54**(11): p. 4125-4139.

24.   Lown, D. and H. Thirsk, *Effect of the solution vapour pressure on the temperature dependence of the dissociation constant of acetic acid in water.* Journal of the Chemical Society, Faraday Transactions 1: Physical Chemistry in Condensed Phases, 1972. **68**: p. 1982-1986.

25.   Peterson, A.A., et al., *Thermochemical biofuel production in hydrothermal media: a review of sub-and supercritical water technologies.* Energy & environmental science, 2008. **1**(1): p. 32-65.

26.   Tyufekchiev, M., et al., *Rapid Depolymerization of Decrystallized Cellulose to Soluble Products via Ethanolysis under Mild Conditions.* ChemSusChem, 2020.

27.   Smith, M.D., et al., *Cosolvent pretreatment in cellulosic biofuel production: effect of tetrahydrofuran-water on lignin structure and dynamics.* Green Chemistry, 2016. **18**(5): p. 1268-1277.

28.   Mellmer, M.A., et al., *Effects of γ-valerolactone in hydrolysis of lignocellulosic biomass to monosaccharides.* Green Chemistry, 2014. **16**(11): p. 4659-4662.

29.   Wohlfarth, C., *Static dielectric constants of pure liquids and binary liquid mixtures: supplement to IV/6*. Vol. 17. 2008: Springer Science & Business Media.

30.   Mellmer, M.A., et al., *Solvent effects in acid-catalyzed biomass conversion reactions.* Angewandte chemie international edition, 2014. **53**(44): p. 11872-11875.